Monolithically Cascaded Micromirror Pair Driven by Angular Vertical Combs for Two-Axis Scanning

Makoto Fujino, Pamela R. Patterson, *Member, IEEE*, Hung Nguyen, *Student Member, IEEE*, Wibool Piyawattanametha, *Student Member, IEEE*, and Ming C. Wu, *Fellow, IEEE*

Abstract—In this work, monolithically cascaded one-axis micromirrors driven by angular vertical comb drives are designed and fabricated. Using W-shaped folded-beam optics, we demonstrate two-axis scanning covering $\pm 6.0°$ two-dimensional area at resonant modes of 7.5 kHz, ± 17 V for a fast-scanning mirror and 1.2 kHz, ± 7 V for a slow-scanning mirror. The experimental results satisfy the requirements for a surveying instrument.

Index Terms—Angular vertical comb drive, micromirror, optical scanner, silicon-on-insulator (SOI) wafer.

I. INTRODUCTION

TWO-AXIS laser-beam steering systems have been used in many optical instruments to perform target search, beam alignment, area sensing, or image display. Currently, cascaded acoustooptic deflectors are used in many optical surveying instruments. Microelectromechanical systems (MEMS) scanners are very attractive candidates for replacing those scanners. They offer many advantages, including lower power consumption, smaller size, and potentially lower cost. Both two-axis and cascaded one-axis MEMS scanners have been reported. Two-axis scanners offer simpler design of optical systems and more compact footprints [1]–[4]. On the other hand, cascaded one-axis scanners offer better mechanical isolation between individual scanning axes, simpler electrical interconnections, simpler fabrication processes, and potentially lower cost. While the footprint of the scanning module is slightly larger, the overall system size (see Fig. 1) remains comparable to those using two-axis scanners. In this paper, we will focus on the cascaded one-axis scanners approach.

Several cascaded micromachined mirror devices have been studied for MEMS confocal microscope and scanning display applications [5]–[9]. Optical surveying instruments require mirrors with reasonably large scan range ($\sim \pm 6°$ mechanical), high resonant frequencies (5–10 kHz for the fast axis), large radius of curvature, and low supply voltage (<50 V). From the packaging point of view, it is also desirable to have the two cascaded scanners monolithically fabricated on a single chip. Vertical comb
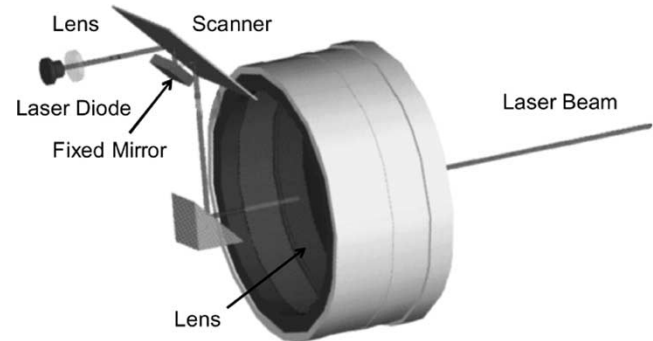
Fig. 1. Schematic illustration of a two-axis micromirror scanner implemented in a surveying instrument.

drive actuators are attractive for for this application because of the large torque [10]–[12].

In this paper, we report on a two-axis MEMS scanner comprising two cascaded one-axis micromirrors for optical surveying instrument applications. The two orthogonal one-axis scanners are monolithically integrated on a silicon-on-insulator (SOI) wafer. We employ angular vertical comb drive (AVC) [4], [13]–[16] actuators for our scanners. It also has a simpler fabrication process, and the comb fingers are inherently self-aligned, since they are patterned in a one-step etching process. We have achieved a resonant scanning with $\pm 6°$ scan range in both axes. The drive voltages are ± 17 V (at 7.5 kHz) and ± 7 V (at 1.2 kHz) for the fast and slow axes, respectively. DC scanning for the slow axis has also been demonstrated ($\pm 6°$ mechanical at 45 V).

II. IMPLEMENTATION OF THE MICROMIRRORS

A. Application and Requirements for the Scanners

The schematic of the optical scanning system in a surveying instrument is shown in Fig. 1. It consists of a laser diode, an imaging lens, a two-axis scanner, a turning mirror, and a collimating lens. We employ a W-shaped folded-beam configuration for our cascaded one-axis scanners so that both MEMS scanners can be integrated on the same wafer.

The target, a highly reflective surface consisting of corner cubes, is located several meters to several kilometers away from the instruments. The required scanning angular range is relatively small, on the order of a few degrees. The angular divergence of the measurement laser beam is typically a few milliradians or narrower. Hence, the target search system needs to resolve several tens of spots in the entire scan range. Raster scanning has been used because the laser beam needs to search
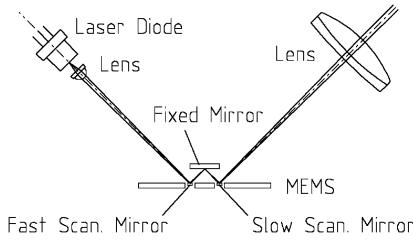
Fig. 2. Schematic illustration of the optical system for two-axis scanning, by using a monolithically cascaded pair of a fast-scanning mirror and a slow-scanning mirror.
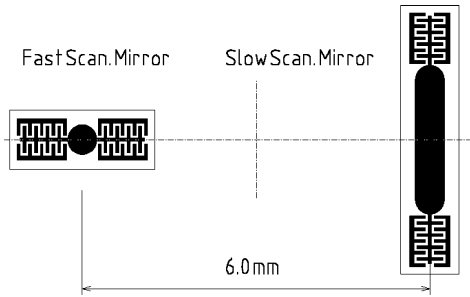

Fig. 3. Schematic top view of chip design.

the entire area within the field of view to find the target. A combination of fast- and slow-scanning deflectors has been employed. However, when the target is closer to the surveying instrument, coarser scanning can find the target. A fast scanner with higher searching rate (approximately over 30 Hz) is desired to track the target. Actuation voltage under 50 V is desired because inexpensive electrical drivers are readily available.

B. Optical Design

The two-axis scanning optical system is illustrated in Fig. 2. The optical system includes a fixed mirror and the combination of a fast-scanning mirror and a slow-scanning mirror, both of which are monolithically fabricated on an SOI wafer. The W-shaped folded-beam geometry allows two-axis scanning in a compact volume. Fig. 3 shows the schematic of the scanner chip (top view). The rotational axes of the mirror pair are perpendicular to each other.

In our design, the spacing between the fast-scanning mirror and the slow-scanning mirror is 6.0 mm. The fast-scanning scanner has a circular shape with 0.4-mm diameter. The slow-scanning mirror has an elongated shape (0.4 mm $\times$ 2.5 mm with circular corners) to accommodate the walkoff of the light beam caused by the first scanner (1.9 mm). The fixed mirror is positioned at 3.0 mm above the scanning mirrors. In the optical system, a laser beam (wavelength $\lambda = 690$ nm, output power $= 1$ mW) illuminates on the fast-scanning mirror at $45°$ and is focused on the fixed mirror. The numerical aperture (NA) of the focused beam is designed to be 0.015. The fixed mirror directs the beam to the slow-scanning mirror. The output beam is collimated by a lens with 50-mm focal length. The size of the outgoing beam is $D = 1.5$ mm in diameter. We designed the scanners to have beam deflection up to $\pm 6.0°$ and the outgoing beam after the collimating lens up to $\pm 0.5°$. To achieve $\pm 6.0°$ optical deflection, the fast-scanning mirror must mechanically tilt $\sin^{-1}(\cos(45°)\sin(\pm 6°)) \approx \pm 4.2°$
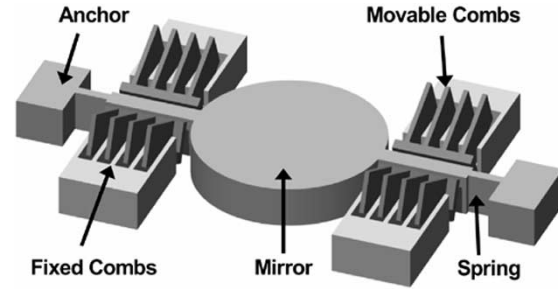

Fig. 4. Schematic illustration of the fundamental architecture of the AVC-driven micromirror.

because of the $45°$ illumination. The slow-scanning mirror only needs $\pm 3.0°$ mechanical angle to achieve $\pm 6.0°$ optical angle. Since beam divergence is $\lambda/D = 0.46 = 0.026°$, the number of resolvable spots of the scanning system is calculated to be $1°/0.026° = 38$.

III. MICROMIRROR SCANNERS

A. Theory

The structure of the micromirrors is schematically shown in Fig. 4. The mirror plate is supported by two torsion beam springs with dimensions of t (thickness), w (width, $w < t$), and l (length). The spring constant is estimated by [17]

$$k = \frac{2Gw^3t}{3l}\left[1 - \frac{192}{\pi^5}\frac{w}{t}\tanh\left(\frac{\pi t}{2w}\right)\right] \qquad (1)$$

where G is shear modulus of the spring material. Taking into account the geometries of the movable part, we can estimate the mass moment of inertia

$$I = I_M + I_C + I_O \qquad (2)$$

where I_M is the moment of inertia of the mirror plate, I_C is that of movable comb fingers, and I_O is from the other structures in the movable body. The resonant frequency of torsion mode is calculated by

$$f = \frac{1}{2\pi}\sqrt{\frac{k}{I}}. \qquad (3)$$

AVC actuators are placed on both sides of the torsion axis. When the dc bias voltage V is applied to the AVC actuators, the mirror tilts by an angle θ due to the torque between fingers. This torque can be written as

$$T(\theta) = \frac{V^2}{2}\frac{\partial C}{\partial \theta} \qquad (4)$$

where C is capacitance between movable combs and fixed combs in AVC actuators. The rotational angle θ is calculated by

$$T(\theta) = k\theta. \qquad (5)$$

The capacitance C can be estimated by the geometry of the AVC actuators such as number of comb pairs N_C, comb finger length L_C, gap spacing between combs, and initial comb angle. To estimate $\partial C/\partial \theta$ accurately and efficiently, we use a hybrid approach that combines a two-dimensional (2-D) finite-element method (FEM) and one-dimensional (1-D) analytical integra-
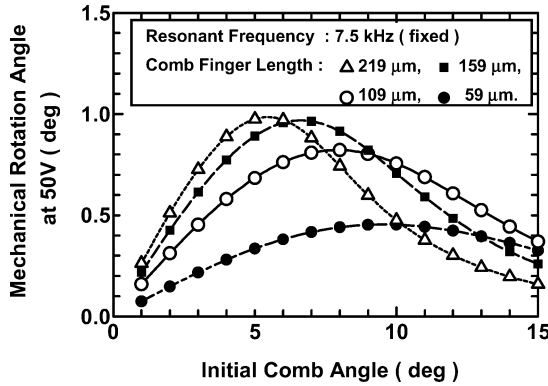
Fig. 5. Mechanical mirror angle versus initial comb angle. In this simulation, mirror size is 0.4 mm in diameter and 25 μm in thickness. Resonant frequency is kept at 7.5 kHz. Applied bias voltage is 50 V. The actuator is composed of three AVC units in each side of the mirror, i.e., 12 units in the device. The AVC unit has 13 fingers 5 μm wide, 25 μm thick, and 3 μm in gap spacing. Comb finger length in the AVC actuator is 59 μm (filled circles), 109 μm (unfilled circles), 159 μm (squares), or 219 μm (triangles). Spacing from AVC hinge to rotation axis of the mirror is 101 μm.

Fig. 6. Mechanical mirror angle versus number of AVC units. In this simulation, mirror size is 0.4 mm in diameter and 25 μm in thickness. Resonant frequency is kept at 7.5 kHz. Applied bias voltage is 50 V. The AVC unit has 13 fingers 5 μm wide, 25 μm thick, and 3 μm in gap spacing. Comb finger length and initial comb angle in the AVC actuator is 59 μm, 9.5° (filled circles), 109 μm, 8.0° (unfilled circles), 159 μm, 6.5° (squares), or 219 μm, 5.5° (triangles) respectively. Spacing from AVC hinge to rotation axis of the mirror is 101 μm.

tion [15], [16], instead of a full three-dimensional (3-D) numerical analysis. The hybrid analysis is suitable for AVC actuators and dramatically reduces the computation time.

B. Simulation for AVC Actuator Design

The geometries and dimensions of the AVC actuator affect the torque and the moment of the inertia of the movable body. The mass moment of inertia of the movable comb fingers is proportional to $N_C L_C^3$. To keep the resonant frequency constant at the desired value, the spring constant should also be proportional to $N_C L_C^3$. On the other hand, the torque generated by the AVC actuators is approximately proportional to $N_C L_C^2$ [16]. Thus, under the constant resonant frequency condition, the mirror angle θ is independent of the number of comb finger pairs N_C when N_C is large and the moment of inertia is dominated by that of the fingers. The mirror angle at a fixed bias voltage will increase initially with L_C when the moment of inertia mainly comes from the mirror, and then decrease with L_C at long finger lengths. There is an optimum L_C for a given mirror dimension.

We find the optimum initial comb angle at a specific applied voltage by using the theory described in Section III-A. Fig. 5 shows the calculated mirror tilt angle at 50-V bias versus the initial comb angle for a variety of finger lengths. The resonant frequency is fixed at 7.5 kHz for all designs. There is an optimum initial comb angle for every comb finger length. At this optimum angle, the mirror rotation is larger for longer finger lengths, but the tolerance of initial comb angle variation becomes tighter. Similarly, Fig. 6 shows the calculated mirror angle at 50-V bias versus the number of AVC units for several combinations of comb finger length and initial comb angles. Each AVC unit has 13 comb fingers with a width of 5 μm, a thickness of 25 μm, and a gap spacing of 3 μm. Indeed, the mirror rotation angle saturates when mass moment of inertia becomes dominated by the comb fingers. We can see from this simulation that a longer comb finger does not always perform better. We designed the comb finger length and initial comb angles, considering the simulation as well as the footprint of the AVC actuators.
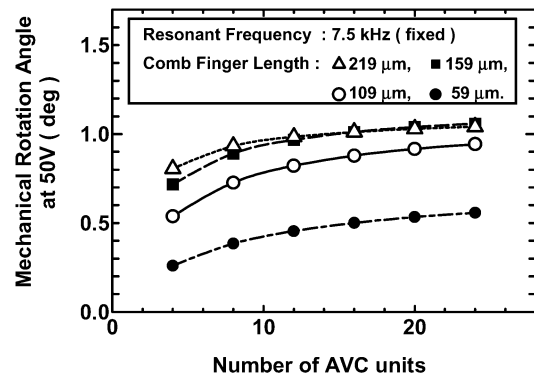
TABLE I
DESIGN PARAMETERS OF THE MIRRORS

	Fast Scan. Mirror	Slow Scan. Mirror
Shape of mirror	Circular	Elongated Circular
Size of mirror	0.4 mm in diameter	0.4 mm $\times$ 2.5 mm
Thickness of mirror, springs, and combs	25 μm	
Length of springs	75 μm	
Length of comb fingers	109 μm	
Width of comb fingers	5 μm	
Gap of combs	3 μm	
Initial comb angles	6 - 8 degrees	

C. Mirror Design

The fast-scanning mirror is driven at its resonant frequency (5–10 kHz). The slow-scanning mirror is designed to operate in dc mode. However, we can also drive it at resonant mode for coarse two-axis scanning when the target is close to the instrument and occupies a large angular area. For full raster scanning, the typical scanning frequency is 150 kHz, which is much smaller than the resonant frequency of the slow-scanning mirror. The design parameters of both scanning mirrors are summarized in Table I.

IV. FABRICATION OF THE MICROMIRRORS

A. Fabrication Process

We fabricated both mirrors monolithically on an SOI wafer with 25-μm-thick device layer, 2-μm-thick buried oxide, and 400-μm-thick substrate. The fabrication process of the mirrors is outlined in Fig. 7.

First, windows were opened by deep reactive ion etching (DRIE) in the 400-μm-thick substrate. Aligning to the backside openings, we simultaneously etched out the 25-μm-thick front-side patterns, including mirror plates, torsion springs, movable combs, and fixed combs by DRIE. Optical inspection from backside allows for precise control of etching time. Photodefinable benzocyclobutene (BCB) (Cyclotene 4024-40,
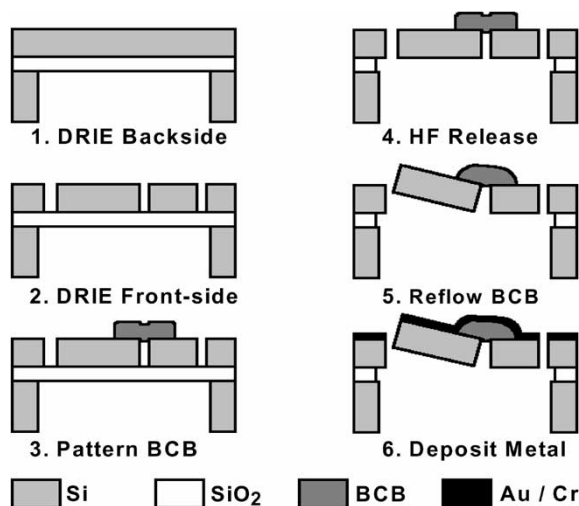
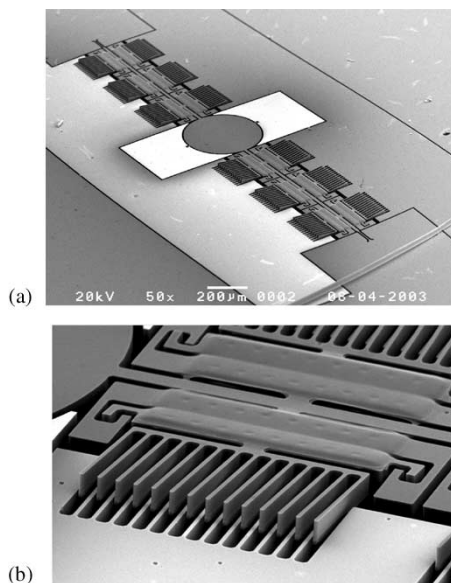Fig. 7.   Fabrication process of the AVC-driven micromirror.

Fig. 8.   (a) SEM of the fast-scanning mirror. (b) Close-up view of the AVC actuator.

Dow Chemical Company, Midland, MI) was spin-coated and patterned as hinges for the AVC actuators. The device was released in 49% hydrofluoric acid and dried with a supercritical dryer. The chip was heated to 400 °C in a furnace. During the thermal reflow, the BCB hinge lifted up the movable combs up to 6°–8° [15]. Finally, 5-nm chromium and 100-nm gold films were deposited by an electron beam evaporator for high-reflectance coating on the mirrors and electrical connection to the movable comb fingers. It is worth noting that the whole process flow includes only two DRIE steps with three masks. Fig. 8 shows the scanning electron micrograph (SEM) of the fabricated fast-scanning mirror.

B. Control of Initial Comb Angle

Since the initial comb angle affects the performance of the scanner, it is important to understand the accuracy and uniformity of the self-assembly process. We found that the tilt angles produced by BCB curing alone have a large variation. To have a
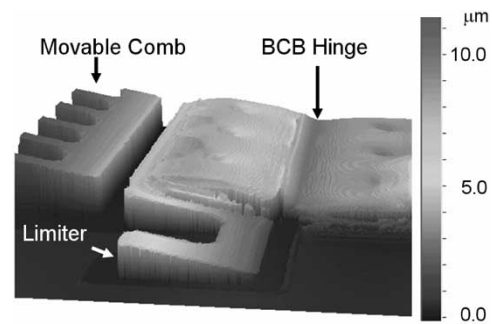

Fig. 9.   Limiter structure controlling the movable comb angles. The 3-D illustration is obtained by white-light interferometric profilometer.
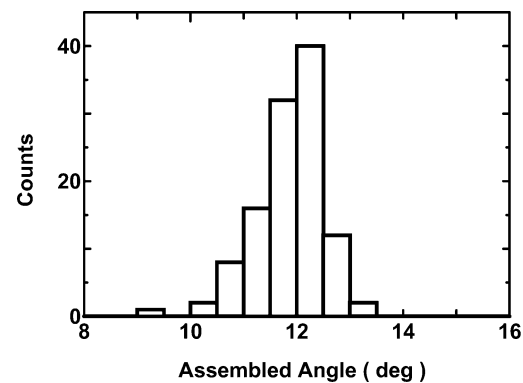

Fig. 10.   Distribution of individual initial comb angles. Average is 11.9°. Root-squre-mean deviation of the distribution is calculated as 0.6°.

tighter control of the comb angle, we have designed some mechanical limiters. The limiter structure is shown in Fig. 9. It is patterned during the same DRIE step when the comb fingers are etched. The gap spacing around the limiter is designed to be very narrow ($\sim 2\ \mu$m). When the comb is lifted up during the BCB curing step, the limiter catches on the sidewalls of the fixed structure and prevents the comb from rotating further. We have designed a test structure to measure the uniformity of the self-assembled angles. The measured angular distribution of 112 AVC units is shown in Fig. 10. The average angle is measured to be 11.9° and the standard deviation is 0.6°. If we design the initial comb angles around the optimum angles shown in Fig. 5, the mirror rotation angle is insensitive to the initial comb angle variation (to $\sim \pm 1°$). There is one drawback of our current limiter structure: the assembled comb angle is sensitive to lateral undercut of the DRIE process. It is also sensitive to change of the gap spacing underneath the BCB (due to shrinkage of the BCB itself). We are currently investigating other limiter structures.

V. EXPERIMENTAL RESULTS

A. Performances of the Scanning Mirrors

We measured mechanical tilt angles of the mirrors under actuation using a white-light interferometric profilometer. Fig. 11 shows the dc performance of the mirrors. The fast- and slow-scanning mirrors tilt $\pm 0.74°$ and $\pm 3.2°$ at 50 V, respectively. To reach $\pm 3°$ in a slow scanner requires a voltage of 45 V, which is less than the 50-V requirement. The theoretically calculated transfer curves are also shown in Fig. 11. Very good agreement between theory and experiments are obtained.
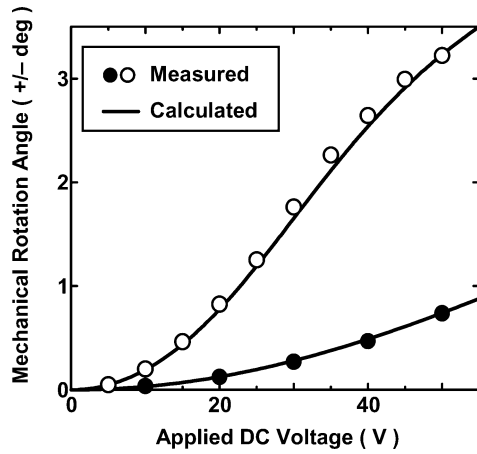
Fig. 11. DC bias voltage dependence of mechanical angle of the mirrors. Dots show the experimental data: the fast-scanning mirror (unfilled circles) and the slow-scanning mirror (filled circles). Solid curves show the calculated data.
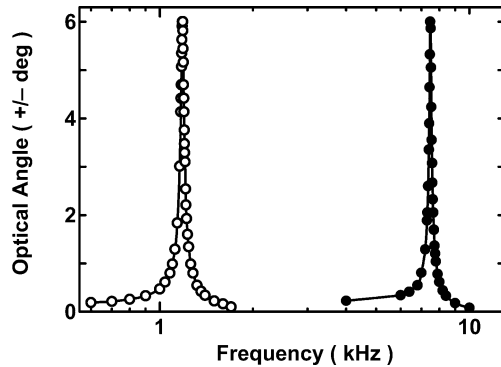

Fig. 12. Frequency dependences of the optical deflection angle. Unfilled circles show the experimental data for the fast-scanning mirror and filled circles show the slow-scanning mirror. The slow-scanning mirror was driven at ± 7-V ac voltage; the fast-mirror was driven at ± 17-V ac voltage.

We also measured the frequency response of the scanners. The experimental setup is designed to mimic the optical design shown in Fig. 2. Instead of using a collimating lens, we used a 2-D position-sensitive detector (PSD) to cover the entire scan area.

The measured frequency responses are shown in Fig. 12. For the fast-scanning mirror, the amplitude of the input sinusoidal signal was fixed at 17 V during the measurement. Scanning angular ranges were estimated from the output of the 2-D PSD on an oscilloscope and the geometries of the measurement system. The maximum amplitude of scanning, 6.0°, was observed at 3.75-kHz signal frequency, which corresponds to mirror vibration frequency of 7.5 kHz (the mirror oscillates twice for each cycle of ac bias). The peak frequency of 7.5 kHz is confirmed by a laser doppler vibrometer. For the slow-scanning mirror, the amplitude of input sinusoidal signal was fixed at 7 V. The maximum amplitude of scanning, 6.0°, was observed at a driving frequency of 600 Hz (mirror frequency = 1.2 kHz). The peak frequency agrees with the measurement by the laser doppler vibrometer.

The quality factors of the scanners are estimated from the shapes of the resonant peaks. They are 68 for the fast-scanning mirror and 44 for the slow-scanning mirror. The radius of curvatures of the mirrors, measured by white-light interferometric

TABLE II
SPECIFICATIONS AND PERFORMANCE OF THE MIRRORS

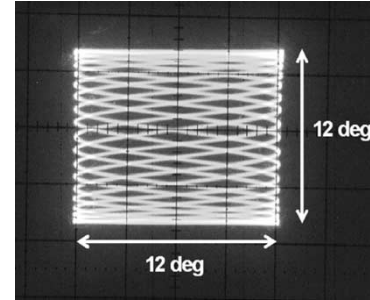|	Fast Scan. Mirror	Slow Scan. Mirror
Size	0.4 mm diameter	0.4mm x 2.5 mm
Flatness	R > 3m	R > 3m
Resonant freq.	7.5 kHz	1.2 kHz
Max. tilt angle (Mechanical)	± 4.2 ° at 17V AC	± 3.0 ° at 45V DC or 7V AC
Max. scan angle (Optical)	± 6.0° at 17V AC	± 6.0 ° at 45V DC or 7V AC
Drive mode	Resonant	DC or Resonant

Fig. 13. Lissajous figure that the scanned light beam drew on a 2-D PSD.

profilometer, are greater than 3 m. The performance of the scanners is summarized in Table II.

B. Demonstration of Two-Axis Scanning

Two-axis scanning was demonstrated by driving both fast- and slow-scanning mirrors at resonance. The fast-scanner is biased at ± 17 V and 7.5 kHz, while the slow axis is biased at ± 7 V, 1.2 kHz. As shown in Fig. 13, the laser beam was steered in $\pm 6.0°$ angular area.

VI. CONCLUSION

We have designed and fabricated a two-axis laser scanner for optical surveying instruments applications. The scanner consists of two cascaded one-axis micromirrors actuated by AVCs. The fast scanner has a circular mirror of 0.4-mm diameter, while the slow scanner has an area of 0.4 mm × 2.5 mm. The micromirrors are made from a 25-μm-thick SOI substrate, and the mirror radii of curvature are larger than 3 m. A W-shaped folded-beam structure is employed to reduce the overall footprint of the scanner as well as allowing both scanners to be monolithically fabricated on the same wafer. Optical scan ranges of $\pm 6°$ before the final collimating lens are obtained in both axes by driving both micromirrors resonantly at 17 V (7.5 kHz) and 7 V (1.2 kHz), respectively. The measured performance agrees very well with the theoretical calculations. The results described in this paper are suitable for applications in optical survey instruments.

REFERENCES

[1] H. Schenk, P. Durr, T. Haase, D. Kunze, U. Sobe, H. Lakner, and H. Kuck, "Large deflection micromechanical scanning mirrors for linear scans and pattern generation," *IEEE J. Select. Topics Quantum Electron.*, vol. 6, pp. 715–722, Sept.–Oct. 2000.

[2] S. Kwon, V. Milanovic, and L. P. Lee, "A high aspect ratio 2D gimbaled microscanner with large static rotation," in *Proc. Int. Conf. Optical MEMS*, 2002, pp. 149–150.

[3] Y. Mizuno, O. Tsuboi, N. Kouma, H. Soneda, H. Okuda, Y. Nakamura, S. Ueda, I. Sawaki, and F. Yamagishi, "A 2-axis comb-driven micromirror array for 3D MEMS switches," in *Proc. Int. Conf. Optical MEMS (OMEMS 2002)*, pp. 17–18.

[4] W. Piyawattanametha, P. R. Patterson, D. Hah, H. Toshiyoshi, and M. C. Wu, "A 2D scanner by surface and bulk micromachined angular vertical comb actuators," in *Proc. IEEE/LEOS Int. Conf. Optical MEMS*, 2003, pp. 93–94.

[5] D. L. Dickensheets and G. S. Kino, "Micromachined scanning confocal optical," *Opt. Lett.*, vol. 21, pp. 764–766, May 1996.

[6] M.-H. Kiang, D. A. Francis, C. J. Chang-Hasnain, O. Solgaard, K. Y. Lau, and R. S. Muller, "Actuated polysilicon micromirrors for raster-scanning displays," in *Proc. 1997 Int. Conf. Solid-State Sensors and Actuators (Transducers'97)*, pp. 323–326.

[7] U. Hofmann, S. Muehlmann, M. Witt, K. Doerschel, R. Schuetz, and B. Wagner, "Electrostatically driven micromirrors for a miniaturized confocal laser scanning microscope," in *Proc. SPIE Conf. Miniaturized Systems With Micro-Optics and MEMS*, vol. 3878, 1999, pp. 29–38.

[8] H. Nguyen, J. G.-D. Su, H. Toshiyoshi, and M. C. Wu, "Device transplant of optical MEMS for out of plane beam steering," in *Tech. Dig. 14th IEEE Int. Conf. Micro Electro Mechanical Systems (MEMS 2001)*, pp. 325–328.

[9] J.-H. Lee, Y.-C. Ko, B.-S. Choi, J.-M. Kim, and D. Y. Jeon, "SOI-fabrication of scanning mirror for laser display," in *Proc. IEEE/LEOS Int. Conf. Optical MEMS*, 2002, pp. 153–154.

[10] H.-M. Jeong, J.-J. Choi, K. Y. Kim, K. B. Lee, J. U. Jeon, and Y. E. G. Park, "Milli-scale mirror actuator with bulk micromachined vertical combs," in *Proc. Int. Conf. Solid-State Sensors and Actuators (Transducers '99)*, pp. 1006–1009.

[11] R. A. Conant, J. T. Nee, K.-Y. Lau, and R. S. Muller, "A flat high-frequency scanning micromirror," in *Tech. Dig. Solid-State Sensor and Actuator Workshop*, 2000, pp. 6–9.

[12] U. Krishnamoorthy and O. Solgaard, "Self-aligned vertical comdrive actuators for optical scanning micromirrors," in *Proc. IEEE/LEOS Int. Conf. Optical MEMS*, 2001, pp. 41–42.

[13] P. R. Patterson, D. Hah, H. Nguyen, R.-M. Chao, H. Toshiyoshi, and M. C. Wu, "A scanning micromirror with angular comb drive actuation," in *Tech. Dig. 15th IEEE Int. Conf. Micro Electro Mechanical Systems (MEMS 2002)*, pp. 544–547.

[14] M. Fujino, P. R. Patterson, H. Nguyen, W. Piyawattanametha, and M. C. Wu, "Cascaded micromirror pair driven by angular vertical combs for two-axis scanning," in *Proc. IEEE/LEOS Int. Conf. Optical MEMS*, 2003, pp. 99–100.

[15] H. D. Nguyen, D. Hah, P. R. Patterson, R. Chao, W. Piyawattanametha, E. K. Lau, and M. C. Wu, "Vertical comb driven tunable capacitor with high tuning capabilities," *J. Microelectromech. Syst.*, vol. 13, pp. 406–413, June 2004.

[16] D. Hah, H. Toshiyoshi, and M. C. Wu, "Design of electrostatic actuators for MOEMS," in *Proc. Symp. Design, Test, Integration and Packaging of MEMS/MOEMS (DTIP 2002)*, pp. 200–207.

[17] S. Timoshenko and J. N. Goodier, *Theory of Elasticity*, 3rd ed. New York: McGraw-Hill, 1970.

Makoto Fujino received the M.S. degree in physics from Kyusyu University in 1992.

He is with the Topcon Corporation, Tokyo, Japan where he has researched integrated optics, diffractive optics, and microoptics. He is currently on leave from Topcon as a Visiting Researcher in Electrical Engineering at the University of California, Los Angeles (UCLA). His research interests include microelectromechanical systems (MEMS), optics, and photonics.

Pamela R. Patterson (S'98–M'03) received the B.S. degree (*cum laude*) from the University of Cincinnati, Cincinnati, OH, in 1978 and the M.S. and Ph.D. degrees in electrical engineering from the University of California, Los Angeles (UCLA), in 1985 and 2003, respectively, completing the dissertation year as a recipient of an Intel Foundation fellowship.

She has held Senior Engineering positions at TRW, Varian, and UCLA, where she helped to establish the Nanoelectronics Research Laboratory from 1994 to 2003. In 2003, she joined HRL Laboratories, LLC, Malibu, CA, as a Research Staff Member and is currently conducting research on hetergeneous integration of semiconductor materials. She has authored or coauthored 14 conference papers, including three invited papers, and contributed a book chapter (coauthored with Dr. M. Wu) in the field of optical MEMS devices. Her research interests are in the area of microfabrication/nanofabrication process design and technology.

Dr. Patterson is a Member of the American Association for the Advancement of Science (AAAS), the American Vacuum Society (AVS), and Eta Kappa Nu.

Hung Nguyen (S'98) received the B.S. degree in physics and the M.S. degree in electrical engineering from the University of California, Los Angeles (UCLA), in 1998 and 2003, respectively. He is currently working toward the Ph.D degree in electrical engineering at UCLA.

His research is mainly in optical microelectromechanical systems (MOEMS) and radio frequency MEMS.

Mr. Nguyen received the Intel Foundation Fellowship for 2004.

Wibool Piyawattanametha (S'98) received the B.Eng. degree (*magna cum laude*) in electronics engineering from King Mongkut's Institute of Technology Ladkrabang (KMITL) in 1994 and the M.Sc. degree in electrical engineering from the University of California, Los Angeles (UCLA), in 1999. He is currently working toward the Ph.D. degree in electrical engineering at UCLA.

From 1994 to 1997, he worked at Schlumberger Limited as a Field Engineer. His research interests include microelectromechanical systems (MEMS), biomedical imaging and sensing systems, and photonics.

Ming C. Wu (S'82–M'83–SM'00–F'02) received the B.S. degree in electrical engineering from National Taiwan University in 1983, and the M.S. and Ph.D. degrees in electrical engineering and computer sciences from the University of California, Berkeley, in 1985 and 1988, respectively.

From 1988 to 1992, he was a Member of Technical Staff at AT&T Bell Laboratories, Murray Hill, NJ. In 1993, he joined the faculty of the Electrical Engineering Department of the University of California, Los Angeles (UCLA), where he is currently a Professor. He is also Director of UCLA's Nanoelectronics Research Facility and Vice Chair for Industrial Relations. He has published over 340 papers, contributed four book chapters, and holds 11 U.S. patents. His current research interests include microelectromechanical systems (MEMS), optical MEMS (MOEMS), biophotonics, microwave photonics, and high-speed optoelectronics.

Dr. Wu was the Founding Cochair for the IEEE LEOS Summer Topical Meeting on Optical MEMS in 1996. The meeting has now evolved into the IEEE LEOS International Conference on Optical MEMS, hosted in Europe, Asia, and the United States. He has also served in program committees of many other conferences, including Optical Fiber Communications (OFC), the Conference on Lasers and Electrooptics (CLEO), the IEEE Conference on Micro Electro Mechanical Systems (MEMS), the LEOS Annual Meetings (LEOS), the International Electron Device Meeting (IEDM), the Device Research Conference (DRC), the International Solid-State Circuit Conference (ISSCC), and Microwave Photonics (MWP). He is a David and Lucile Packard Foundation Fellow (1992–1997).